



Chronic Activation of LXR α Sensitizes Mice to Hepatocellular Carcinoma

Yang Xie ¹, Runzi Sun,² Li Gao,^{1,3} Jibin Guan,¹ Jingyuan Wang,¹ Aaron Bell,⁴ Junjie Zhu,¹ Min Zhang,¹ Meishu Xu,¹ Peipei Lu,¹ Xinran Cai,¹ Songrong Ren,¹ Pengfei Xu,¹ Satdarshan P. Monga ^{4,5}, Xiaochao Ma,¹ Da Yang,¹ Yulan Liu,³ Binfeng Lu,² and Wen Xie^{1,6}

The oxysterol receptor liver X receptor (LXR) is a nuclear receptor best known for its function in the regulation of lipid and cholesterol metabolism. LXRs, both the α and β isoforms, have been suggested as potential therapeutic targets for several cancer types. However, there was a lack of report on whether and how *LXR α* plays a role in the development of hepatocellular carcinoma (HCC). In the current study, we found that systemic activation of *LXR α* in the *VP-LXR α* knock-in (*LXR α KI*) mice or hepatocyte-specific activation of *LXR α* in the *VP-LXR α* transgenic mice sensitized mice to liver tumorigenesis induced by the combined treatment of diethylnitrosamine (DEN) and 3,3',5,5'-tetrachloro-1,4-bis (pyridyloxy) benzene (TCPOBOP). Mechanistically, the *LXR α* -responsive up-regulation of interleukin-6 (IL-6)/signal transducer and activator of transcription 3 (STAT3) signaling pathway and the complement system, and down-regulation of bile acid metabolism, may have contributed to increased tumorigenesis. Accumulations of secondary bile acids and oxysterols were found in both the serum and liver tissue of *LXR α* activated mice. We also observed an induction of monocytic myeloid-derived suppressor cells accompanied by down-regulation of dendritic cells and cytotoxic T cells in DEN/TCPOBOP-induced liver tumors, indicating that chronic activation of *LXR α* may have led to the activation of innate immune suppression. The HCC sensitizing effect of *LXR α* activation was also observed in the *c-MYC* driven HCC model. **Conclusion:** Our results indicated that chronic activation of *LXR α* promotes HCC, at least in part, by promoting innate immune suppressor as a result of accumulation of oxysterols, as well as up-regulation of the IL-6/Janus kinase/STAT3 signaling and complement pathways. (*Hepatology Communications* 2022;6:1123-1139).

Hepatocellular carcinoma (HCC) is the major form of primary liver cancers and the second-most lethal cancer after the pancreatic cancer. The classical risk factors for HCC include viral infection and liver toxins.^(1,2) The increase in nonalcoholic fatty liver disease (NAFLD), together with metabolic syndrome and obesity, amplifies the risk of liver

cancer. NAFLD is expected to become a leading cause of liver cancer in Western countries,⁽³⁾ suggesting the critical role of lipid disorder in the development of HCC. Commonly used rodent models of HCC include those induced by the combined treatment of the tumor initiator diethylnitrosamine (DEN) and tumor promoter 3,3',5,5'-tetrachloro-1,4-bis

Abbreviations: CC, cholangiocarcinoma; Cyp, cytochrome P450; CXCR2, CXC chemokine receptor 2; DEN, diethylnitrosamine; FABP, fatty acid binding protein; FXR, farnesoid X receptor; GMP, granulocyte and macrophage progenitor cell; GSEA, gene-set enrichment analysis; HC, 20-hydroxycholesterol; HCC, hepatocellular carcinoma; HDCA, hydoxycholeolic acid; IL-6, interleukin-6; JAK, Janus kinase; LAP, liver-enriched activator protein; LXR, liver X receptor; MDSC, myeloid-derived suppressor cell; mRNA, messenger RNA; PCR, polymerase chain reaction; RNA-seq, RNA-sequencing; STAT3, signal transducer and activator of transcription 3; TCGA, The Cancer Genome Atlas; TCPOBOP, 3,3',5,5'-tetrachloro-1,4-bis (pyridyloxy) benzene; T-DCA, taurodeoxycholic acid; T-UDCA, tauroursodeoxycholic acid; UPLC, ultra-performance liquid chromatography; WT, wild-type; ω -MCA, ω -muricholic acid.

Received October 4, 2021; accepted November 18, 2021.

Additional Supporting Information may be found at onlinelibrary.wiley.com/doi/10.1002/hep4.1880/supinfo.

Supported by the National Institutes of Health (DK117370 and ES030429 to W.X.).

© 2022 The Authors. *Hepatology Communications* published by Wiley Periodicals, Inc., on behalf of the American Association for the Study of Liver Diseases. This is an open access article under the terms of the Creative Commons Attribution-NonCommercial-NoDeriv License, which permits use and distribution in any medium, provided the original work is properly cited, the use is non-commercial and no modifications or adaptations are made.

View this article online at [wileyonlinelibrary.com](https://onlinelibrary.wiley.com).

DOI 10.1002/hep4.1880

Potential conflict of interest: Nothing to report.

(pyridyloxy) benzene (TCPOBOP),⁽⁴⁾ or the c-MYC oncogene.⁽⁵⁾

The oxysterol receptors liver X receptor α (*LXR α*) and *LXR β* play a central role in the regulation of lipid and cholesterol metabolism. *LXR α* is highly expressed in the liver, but it is also found in adipose tissue, intestines, kidneys and macrophages, whereas *LXR β* expression is detectable in most tissues.⁽⁶⁾ LXRs have been proposed to be therapeutic targets for several cancer types, including breast cancer,^(7,8) prostate cancer,⁽⁹⁾ and HCC,⁽¹⁰⁻¹⁴⁾ through multiple pathways, ranging from promoting cholesterol metabolism⁽⁷⁻⁹⁾ to cross-talk with transforming growth factor β ,^(11,12) and dampening innate immune responses.⁽¹⁵⁾ More specifically, it has been reported that activation of LXRs inhibited tumor cell proliferation by promoting cholesterol catabolism and reducing intracellular cholesterol content.^(14,16) A recent study showed that activation of *LXR β* reduced myeloid-derived suppressor cells (MDSCs), an immature myeloid heterogeneous population markedly expanded and accumulated in the tumor microenvironment, in murine models and in patients treated the small-molecule LXR agonist RGX-104.⁽¹⁵⁾ However, the cancer inhibitory effect of LXR activation remains controversial. For example, a recent report showed that pharmacological inhibition of LXR using the synthetic LXR inverse agonist SR9243 induced tumor destruction, primarily through stimulation of CD8+ T-cell cytotoxic activity and mitochondrial metabolism *in vitro* and *in vivo*.⁽¹⁷⁾

LXRs are also known as anti-inflammatory transcription factors and physiological regulators of innate and adaptive immune responses. Activation of LXRs resulted in transcriptional silencing of the pro-inflammatory transcription factor nuclear factor kappa B⁽¹⁸⁾ and dampening of the antitumor responses

of dendritic cells (DCs).⁽¹⁹⁾ *LXR α* null mice were reported to be more susceptible to bacterial infection and showed accelerated apoptosis.⁽²⁰⁾ Knowing chronic inflammation is a risk factor for cancers, the anti-inflammatory activity of LXRs may have also contributed to their antitumor activities.

Most of the reported effects of LXRs on cancers have relied on the short-term use of LXR agonists or antagonists. Because LXR modulators are not typical cytotoxic chemotherapeutic agents, it is conceivable that their use in the clinical settings is likely to be chronic. As such, it is necessary to evaluate the effect of chronic activation of LXRs on cancers, including HCC.

In this study, we were surprised to find that chronic activation of *LXR α* systemically, or specifically in hepatocytes, sensitized mice to chemical and oncogenic models of HCC.

Materials and Methods

CHEMICALS

DEN and TCPOBOP were purchased from Sigma-Aldrich (St. Louis, MO).

ANIMALS AND MOUSE MODELS OF HCC

The creation and characterization of *VP-LXR α* knock-in (*LXR α KI*)⁽²¹⁾ and fatty acid binding protein (*FABP*)-*VP-LXR α* transgenic mice⁽²²⁾ were previously reported. To establish chemical-induced HCC, 5-week-old male mice were injected with a single dose of DEN (90 mg/kg body weight, intraperitoneally).

ARTICLE INFORMATION:

From the ¹Center for Pharmacogenetics and Department of Pharmaceutical Sciences, University of Pittsburgh, Pittsburgh, PA, USA; ²Department of Immunology, University of Pittsburgh, Pittsburgh, PA, USA; ³Department of Gastroenterology, Peking University People's Hospital, Beijing, China; ⁴Division of Experimental Pathology, Department of Pathology, University of Pittsburgh, Pittsburgh, PA, USA; ⁵Pittsburgh Liver Research Center, University of Pittsburgh Medical Center and University of Pittsburgh School of Medicine, Pittsburgh, PA, USA; ⁶Department of Pharmacology and Chemical Biology, University of Pittsburgh, Pittsburgh, PA, USA.

ADDRESS CORRESPONDENCE AND REPRINT REQUESTS TO:

Wen Xie, M.D., Ph.D.,
Center for Pharmacogenetics and Department of Pharmaceutical
Sciences, University of Pittsburgh School of Pharmacy

Pittsburgh, PA 15261, USA
E-mail: wex6@pitt.edu
Tel.: +412-648-9941

A week after the DEN injection, mice received biweekly intraperitoneal injections of TCPOBOP (3 mg/kg body weight) for 14 weeks.⁽⁴⁾ Mice were sacrificed and tissues were harvested 2 weeks after the last injection of TCPOBOP. The tet-off liver-enriched activator protein (*LAP*)–*MYC* transgenic mice have been described previously.⁽²³⁾ *LAP-MYC/LXR α KI* mice were generated by breeding the *LAP-MYC* transgene into the *LXR α KI* background. *LAP-MYC* and *LAP-MYC/LXR α KI* mice were maintained with drinking water containing 2 mg/mL of doxycycline (dox) to silence the transgene, and the expression of *MYC* was induced by withdrawing dox. All mice were maintained in C57/BL6 background, and only male mice were used in this study due to their higher sensitivity to experimental HCC. The use of mice in this study has complied with all relevant federal guidelines and institutional policies, and has been approved by the University of Pittsburgh Institutional Animal Care and Use Committee.

HISTOLOGY AND IMMUNOHISTOCHEMISTRY

The liver tissues were freshly harvested and fixed in 10% neutral-buffered formalin for 24 hours. The tissues were histologically processed, embedded in paraffin, sectioned at 4 μ m, and stained with hematoxylin and eosin (H&E) for general histology. For CD45 and Ki67 immunostaining, de-paraffinized sections were incubated with anti-CD45 antibody (Cat#70257) from Cell Signaling (Danvers, MA) at 1:100 dilution, or anti-Ki67 antibody from Abcam (Cambridge, MA) at 1:200 dilution overnight at 4°C. The antibody signals were visualized by peroxidase reaction using 3,3'-diaminobenzidine as the chromogen. Hematoxylin was used as a nuclear counterstain. At least three mice were used for each treatment group, and for each sample at least four noncontiguous regions were photographed and analyzed. Quantification of Ki67 positive stain was calculated by ImageJ.⁽²⁴⁾

RNA-SEQUENCING ANALYSIS

RNA-sequencing (RNA-seq) was performed at the Health Sciences Sequencing Core at the Children's Hospital of Pittsburgh. Gene expression was analyzed by gene-set enrichment analysis.⁽²⁵⁾

REAL-TIME REVERSE-TRANSCRIPTION POLYMERASE CHAIN REACTION

Total RNA was extracted from tissues using TRIzol reagent. Total RNA was treated with RNase-free DNase I and reverse-transcribed into single-stranded complementary DNA. SYBR Green-based real-time polymerase chain reaction (PCR) was performed with the ABI 7300 real-time PCR System. Data were normalized against the housekeeping gene cyclophilin. Relative gene expression was calculated using the $\Delta\Delta$ CT method, in which fold difference was calculated using the expression $2^{-\Delta\Delta$ CT}. The primer sequences are provided in Supporting Table S1.

FLOW CYTOMETRY AND FLUORESCENCE-ACTIVATED CELL SORTING

Tumor dissection and digestion were performed as described.⁽²⁶⁾ In brief, tissue samples were ground and digested with 0.25 mg/mL Liberase TL (Roche, Indianapolis, Indiana) and 0.3 mg/mL DNase (Fisher Scientific, Hampton, NH) for 30 minutes at 37°C. Single-cell suspensions were filtered through a 100- μ m cell strainer. Multiparameter staining was used to identify the immune cell populations as follows: (1) CD8⁺ T cells (CD45⁺ CD8⁺) and CD4⁺ T cells (CD45⁺ CD4⁺); (2) macrophage M1 type (CD45⁺CD11b⁺ F4/80⁺ CD206⁻) and macrophage M2 type (CD45⁺ CD11b⁺ F4/80⁺ CD206⁺); (3) DCs (CD45⁺MHCII⁺ CD11b⁺ Gr-1⁻ F4/80⁻ CD103⁺); (4) MDSCs (monocytic myeloid-derived suppressor cells [Mo-MDSCs]: CD45⁺ CD11b⁺ Gr-1^{int}; granulocytic-MDSCs [G-MDSCs]: CD45⁺ CD11b⁺ G-1^{high}); and (5) granulocyte and macrophage progenitor cells (GMPs) (CD45⁺Lin⁻c-Kit^{high}Sca1⁻Fc γ R1I/III^{high}CD34⁺). The stained cells were applied for data acquisition using Cytex Aurora flow cytometer (Cytex Biosciences, Fremont, CA) and analyzed by FlowJo software (TreeStar Inc., San Carlos, CA). The fluorescence-activated cell sorting analysis of MDSCs was conducted as previously reported.⁽²⁷⁾ Single cells were labeled with anti-CD11b-APC, anti-Ly6C-fluorescein isothiocyanate, and anti-GR-1-PE. G-MDSCs are defined as CD11b⁺Gr-1^{high}Ly6C^{low}, and Mo-MDSCs are defined as CD11b⁺Gr-1^{int}Ly6C^{low}. All of the antibodies used for flow cytometry are listed in Supporting Table S2.

ULTRA-PERFORMANCE LIQUID CHROMATOGRAPHY–MASS SPECTROMETRY ANALYSIS OF BILE ACIDS AND OXYSTEROLS

The serum and liver bile acids were extracted and measured following the method described previously.⁽²⁸⁾ Briefly, 50 μ L of serum sample was mixed with 150 μ L of methanol, followed by vortexing for 30 seconds and centrifugation at 15,000g for 10 minutes. Liver samples were homogenized in water (100 mg tissue in 400 μ L water), and then a 200- μ L aliquot of methanol was added to 100 μ L of liver homogenate. After vortex and centrifugation at 15,000g for 20 minutes, the supernatant was transferred to a new Eppendorf tube for a second centrifugation. A total of 2 μ L of the supernatant was injected onto the ultra-performance liquid chromatography (UPLC) and quadrupole time-of-flight mass spectrometry system for metabolite analysis. Chromatographic separation of bile acids was performed on an Acquity UPLC BEH C18 column (2.1 \times 100 mm, 1.7 μ m; Waters Corporation, Milford, MA) using acetonitrile/water containing 0.1% formic acid as the mobile phase.⁽²⁹⁾ The detailed parameters for mass spectrometry were the same as previously reported.⁽³⁰⁾

The liver contents of oxysterols were measured by the Duke University Proteomics and Metabolomics Shared Resources using a customized UPLC electrospray ionization tandem mass spectrometry method, allowing chromatographic resolution of the isobaric hydroxycholesterol species. The extracting and measurement method of oxysterols involve alkaline hydrolysis of lipid esters followed by solid phase extraction (HyperSep C18 SPE [200 mg]) before liquid chromatography–mass spectrometry analysis. The detailed methods for oxysterol measurements were described previously.⁽³¹⁾ Liver concentrations of 20-hydroxycholesterol (HC), 22(R)-HC, 22(S)-HC, 24(R/S)-HC, 25-HC, 27-HC, 7 α / β -HC, and cholesterol concentrations were semi-quantitative, calculated based on a ratio to each internal standard (stable-isotope dilution).

STATISTICAL ANALYSIS

Results are expressed as mean \pm SEM. Differences between two individual groups were determined by

Student's *t* test. Differences between multiple groups were evaluated using two-way analysis of variance followed by *post-hoc* multiple comparison according to the Tukey's test. Pearson chi-square and Fisher exact were used for between-group comparisons for tumor incidence. Statistical significance was accepted at $P < 0.05$.

Results

INCREASED EXPRESSION OF LXR α IN PATIENTS WITH HCC IS ASSOCIATED WITH POOR SURVIVAL

To determine the expression of LXR in human HCC, we analyzed The Cancer Genome Atlas (TCGA) HCC data sets, including gene-expression profile and clinical features through GEPIA at <http://gepia.cancer-pku.cn/>.⁽³²⁾ The transcripts of both *LXR α* and *LXR β* tended to be higher in HCC compared with normal liver tissues, but the difference did not reach statistical significance (Fig. 1A). The higher expression of both *LXR α* and *LXR β* was associated with lower survival rates of patients with HCC, but the association with *LXR α* expression was statistically more significant (Fig. 1B). To determine the expression of *LXR α* and *LXR β* in different liver cancer types and disease stages, two online Gene Expression Omnibus data sets downloaded from Oncomine (<https://oncomine.org>) were analyzed. Analysis of GSE15765 revealed that the messenger RNA (mRNA) expression of *LXR α* was significantly higher in HCC tumors than in cholangiocarcinoma (CC) tumors (Fig. 1C, top panel), but the expression of *LXR β* was not different between HCC and CC (Fig. 1C, bottom panel). Analysis of GSE6764 showed that the expression of *LXR α* decreased in cirrhosis and pre-neoplastic hyperplastic livers compared with normal livers, after which the expression of *LXR α* increased as the disease progresses, leading to elevated expression of *LXR α* in advanced HCC compared to hyperplastic livers (Fig. 1D, left panel). In the same cohort of patients, the disease stages had little effect on the expression of *LXR β* (Fig. 1D, right panel). These results suggest that elevated expression of *LXR α* was associated with the pathogenesis and poor prognosis of human HCC.

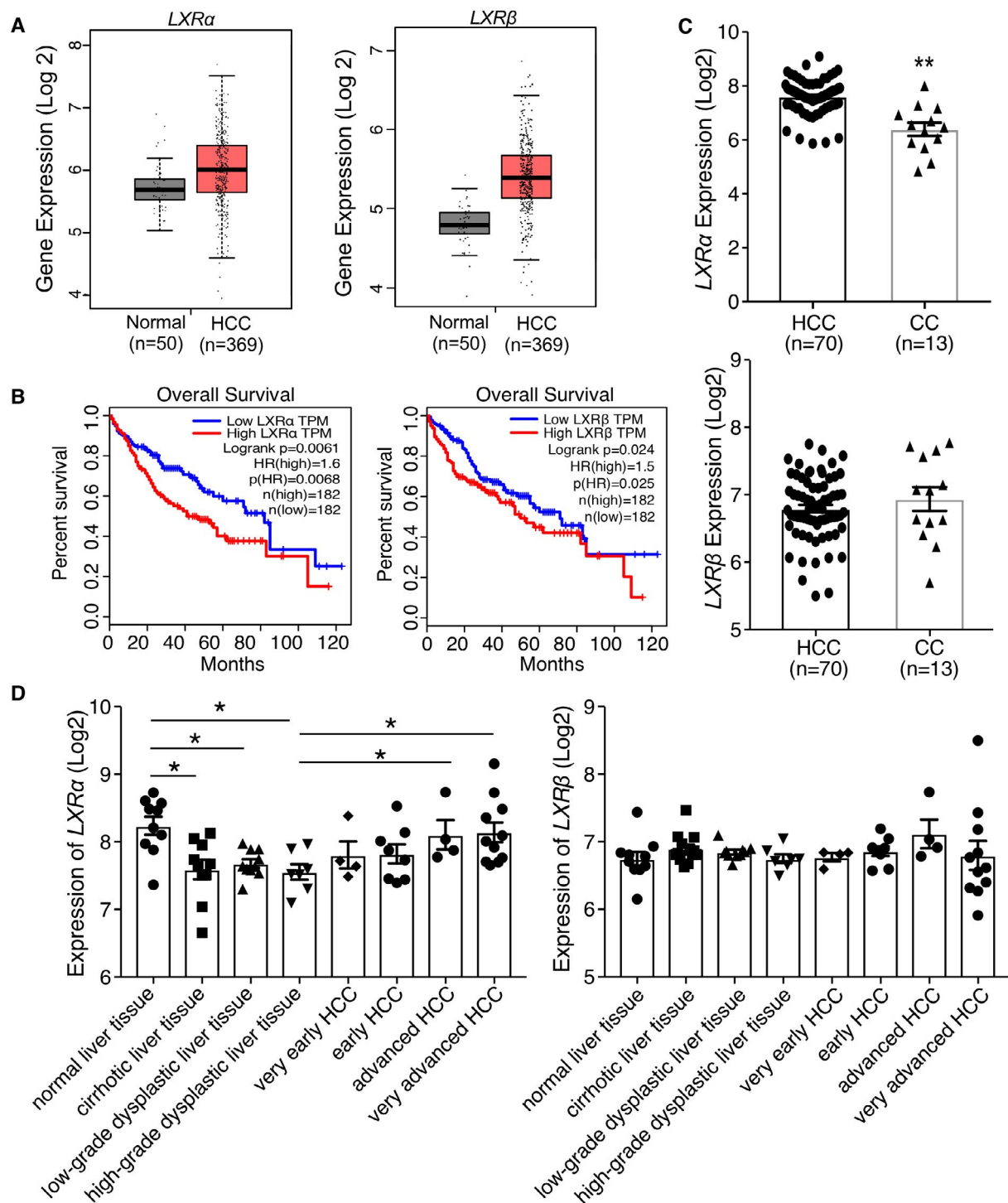


FIG. 1. Increased expression of *LXRα* in patients with HCC is associated with poor survival. (A) Analysis of *LXRα* and *LXRβ* gene expression in the TCGA HCC data set (normal control n = 50; HCC n = 369). (B) The overall survival curves of patients with HCC of high (n = 182) (high cutoff > 50% median) or low (n = 182) (low cutoff < 50% median) expression of *LXRα* or *LXRβ*. (C) Comparative expression of *LXRα* and *LXRβ* in patients with HCC (n = 70) and CC (n = 13). (D) Comparative expression of *LXRα* and *LXRβ* in patients with HCC of different stages (normal liver tissue n = 10; cirrhotic liver tissue n = 13; low-grade dysplastic liver tissue n = 10; high-grade dysplastic liver tissue n = 7; very early HCC n = 4; early HCC n = 8; advanced HCC n = 4; and very advanced HCC n = 11). **P* < 0.05; ***P* < 0.01; the comparisons are labeled.

CHRONIC ACTIVATION OF LXR α SENSITIZES MICE TO CHEMICAL-INDUCED HCC

We then used LXR α gain-of-function models, *VP-LXR α* knock-in (*LXR α KI*) mice and *VP-LXR α* transgenic mice, to investigate the role of LXR α activation in liver carcinogenesis. As outlined in Fig. 2A, the *LXR α KI* mice were created by knocking the constitutively activated *VP-LXR α* into the endogenous *LXR α* gene locus,⁽²¹⁾ whereas the *VP-LXR α* transgenic mice bear hepatocyte-specific expression of *VP-LXR α* under the control of the FABP gene promoter.⁽²²⁾ *VP-LXR α* was constructed by fusing the VP16 activation domain of the herpes simplex virus to the amino terminus of mouse LXR α sequence.

We initially used the 36 weeks DEN-induced liver carcinogenesis model⁽³³⁾ as outlined in Supporting Fig. S1A, but found the DEN alone regimen was not efficient to induce HCC in wild-type (WT), *LXR α KI*, or *VP-LXR α* mice (Supporting Fig. S1B). The lack of tumor formation in the DEN alone model was consistent with a previous report.⁽³³⁾ TCPOBOP, a constitutive androstane receptor (CAR) agonist that promotes hepatocyte proliferation, is an established liver-cancer promoter following the initiation of DEN.⁽³⁴⁾ We then subjected mice to the DEN/TCPOBOP model of liver cancer.⁽⁴⁾ In this model, mice were injected with a single intraperitoneal dose of DEN (90 mg/kg body weight) at 5 weeks of age, followed by biweekly intraperitoneal injections of TCPOBOP (3 mg/kg body weight) for 16 weeks as outline in Fig. 2B. The expression of the transgenic *VP-LXR α* in the nontumor and tumor tissues of *LXR α KI* and *VP-LXR α* mice was confirmed by real-time PCR, whereas the expression of *LXR β* was not affected by the transgene (Fig. 2C). Compared with their WT counterparts, DEN/TCPOBOP-treated *LXR α KI* and *VP-LXR α* mice showed higher tumor incidence (Fig. 2D) and multiplicity (Fig. 2E), as supported by the gross appearance of the liver (Fig. 2F) and H&E staining of liver sections (Fig. 2G). Immunohistochemical staining of Ki67 also showed a more robust proliferation of tumor cells in *LXR α KI* and *VP-LXR α* mice (Fig. 2H). The tumor multiplicity (Fig. 2D) and Ki67 staining (Fig. 2G) were not statistically different between the *LXR α KI* and *VP-LXR α* mice. As expected, the hepatic expression of *Cyp2b10*, the primary target gene of CAR, was up-regulated

in TCPOBOP-treated mice of all three genotypes (Supporting Fig. S1C).

Interestingly, *LXR α* ablation had little effect on animal's sensitivity to the DEN/TCPOBOP model of HCC, as evidenced by unchanged liver to body weight ratio (Supporting Fig. S2A), tumor incidence (Supporting Fig. S2B), and tumor multiplicity (Supporting Fig. S2C). It remains to be determined whether there will be a compensatory regulation of LXR β in the *LXR α* null mice, and if so, whether this compensatory regulation of LXR β will have functional consequence in the absence of exogenously added LXR agonists *in vivo*.

CHRONIC ACTIVATION OF LXR α UP-REGULATES PATHWAYS ASSOCIATED WITH INNATE IMMUNE SUPPRESSION, BUT DOWN-REGULATES THE BILE ACID METABOLISM PATHWAY IN CHEMICAL-INDUCED HCC

To understand the mechanism by which activation of LXR α sensitizes mice to DEN/TCPOBOP-induced HCC, we performed RNA-seq analysis on liver tumors derived from WT, *LXR α KI*, and *VP-LXR α* mice. There were eight pathways commonly up-regulated in both *LXR α KI* and *VP-LXR α* mice that are known to be involved tumor progression and immune responses (Fig. 3A). Among the commonly up-regulated pathways, our gene-set enrichment analysis (GSEA) analysis validated the activations of interleukin-6 (IL-6)/Janus kinase (JAK)/signal transducer and activator of transcription 3 (STAT3) signaling (Fig. 3B) and complement (Fig. 3C) pathways, both of which have been reported to play important roles in innate immune suppression, including the recruitment of MDSCs to reduce cytotoxic T-cell responses, as well as induction of tumor metastasis and proliferation.^(35,36) The up-regulation of representative genes in the IL6/JAK/STAT3 signaling pathway (Fig. 3D) and complement pathway (Fig. 3E) were validated by real-time reverse-transcription PCR.

Meanwhile, there were five metabolism-related pathways commonly down-regulated in DEN/TCPOBOP-treated *LXR α KI* and *VP-LXR α* mice, among which the down-regulation of bile

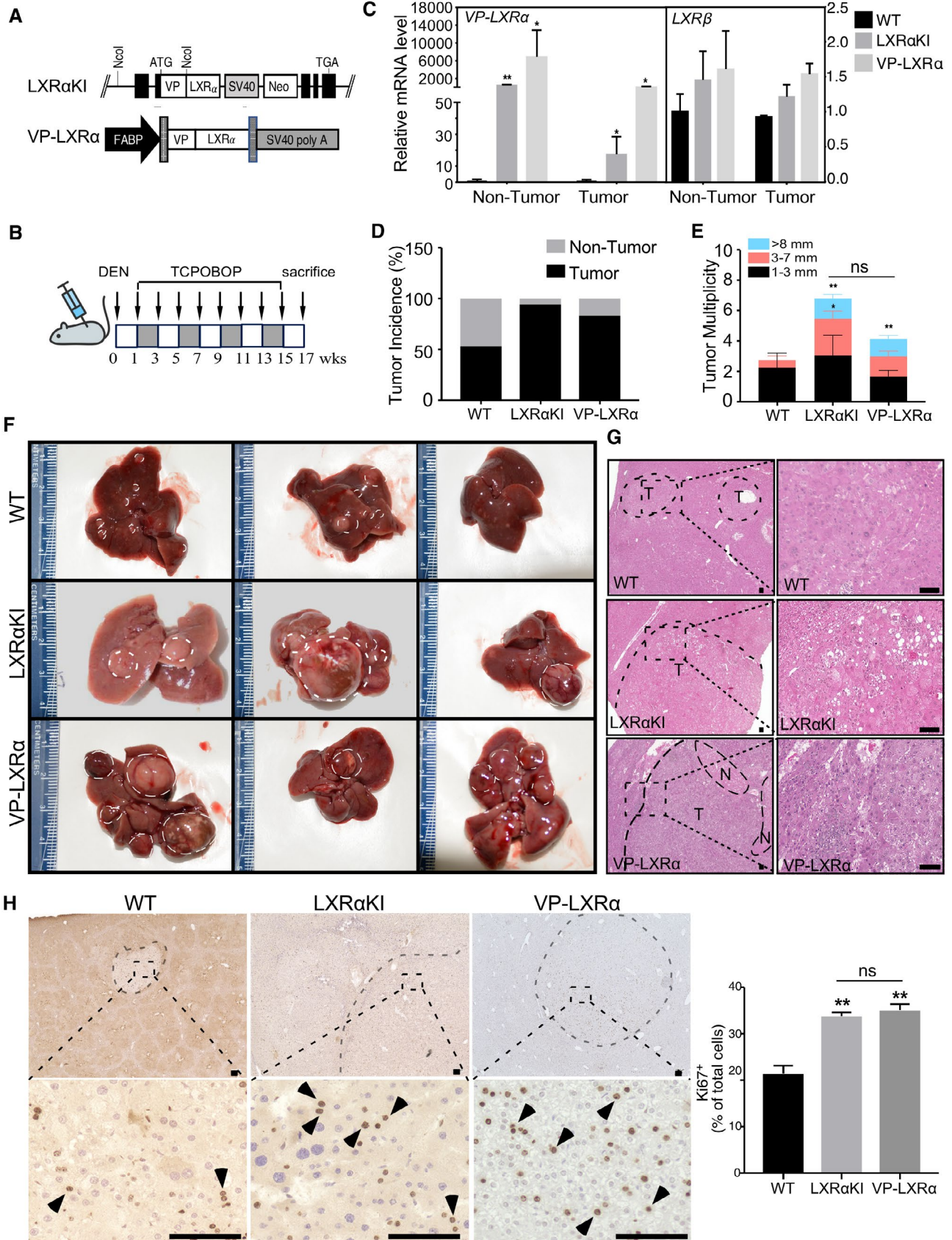


FIG. 2. Chronic activation of LXR α sensitizes mice to chemical-induced HCC. (A) Schematic representation of the *VP-LXR α* knock-in (*LXR α KI*) mice, in which *VP-LXR α* was knocked into the endogenous *LXR α* gene locus, and *FABP-VP-LXR α* transgenic mice expressing *VP-LXR α* in the hepatocytes under the control of hepatocyte-specific *FABP* gene promoter. (B) Scheme of the DEN/TCPOBOP model of HCC. Five-week-old male mice were injected with a single dose of DEN (90 mg/kg body weight, intraperitoneally). A week after the DEN injection, mice received biweekly intraperitoneal injections of TCPOBOP (3 mg/kg body weight) for 14 weeks, and mice were sacrificed 2 weeks after the last injection of TCPOBOP. (C) The expression of *VP-LXR α* and *LXR β* in nontumor and tumor tissues was measured by real-time PCR. (D,E) Liver tumor incidence (D) and multiplicity (E) were calculated in WT, *LXR α KI*, and *VP-LXR α* mice. (F) Gross appearance of the livers following the completion of the DEN/TCPOBOP treatment. Dashed circles indicate tumor nodules. (G) Liver histology was analyzed by H&E staining. Shown on the right are magnified areas of corresponding smaller boxes on the left. Bar is 100 μ m. (G) Tumor cell proliferation was analyzed by immunohistochemistry staining of Ki67. Shown on the bottom are magnified areas of corresponding smaller boxes on the top. Arrowheads indicate Ki67-positive cells. Bar is 100 μ m. Shown on the right is the quantification of the Ki67-positive cells within the tumor areas. * $P < 0.05$; ** $P < 0.01$. Abbreviations: ATG, anti-thymocyte globulin; ns, statistically not significant, compared with the WT group, or the comparisons are labeled; and TGA, transglutaminase IgA.

acid metabolism pathway was ranked at the top (Fig. 3F). GSEA analysis further confirmed the down-regulation of the bile acid metabolism pathway in *LXR α KI* and *VP-LXR α* mice (Fig. 3G), suggesting a potential role of LXR α responsive regulation of the bile acid metabolism in the development of HCC.

CHRONIC ACTIVATION OF LXR α ACCUMULATES PRO-HCC BILE ACID SPECIES AND OXYSTEROLS IN CHEMICAL-INDUCED HCC

Because our RNA-seq results suggested a dysregulation of the bile acid metabolism pathway (Fig. 4A), we wanted to validate the LXR α responsive changes in the expression of key enzymes involved in the bile acid metabolism. The up-regulation of cytochrome P450 (*Cyp*) *7a1* and down-regulation of *Cyp7b1* and *Cyp8b1* in tumors derived from *VP-LXR α* mice were verified by real-time PCR. A similar pattern of regulation was observed in *LXR α KI* mice (Fig. 4B, top panel). The LXR α -responsive induction of *Cyp7a1* and suppression of *Cyp7b1* were consistent with our previous report.^(22,37) Interestingly, besides a robust induction of *Cyp7a1*, a significant induction of *Cyp8b1* was also observed in adjacent nontumor tissue of *LXR α KI* and *VP-LXR α* mice (Fig. 4B, bottom panel). Analysis of the TCGA data sets by GEPIA showed a significant up-regulation of *CYP7A1*, down-regulation of *CYP8B1*, and a trend of down-regulation in *CYP7B1* in human HCC (Fig. 4C), suggesting that the dysregulation of bile acid metabolism was conserved in patients with HCC.

When bile acid levels in the serum (Fig. 4D) and nontumor liver tissues (Fig. 4E) were measured, we

found increased concentrations of multiple species of unconjugated and conjugated bile acids in *LXR α KI* and *VP-LXR α* mice, consistent with the induction of the bile acid synthesis rate-limiting enzyme *Cyp7a1*, as well as the suppression of a battery of genes involved in the bile acid metabolism, such as farnesoid X receptor (FXR, encoded by gene NR1H4) and small heterodimer partner (encoded by gene NR0B2), which are transcriptional factors mediating the negative-feedback regulation of bile acid synthesis (Fig. 4A). Among the bile acid species whose levels were elevated in *LXR α KI* and *VP-LXR α* mice, ω -muricholic acid (ω -MCA), hyodeoxycholic acid (HDCA), taurodeoxycholic acid (T-DCA), and tauroursodeoxycholic acid (T-UDCA) are secondary bile acids known to promote HCC.^(38,39) The accumulation of FXR antagonist bile acids, including T- α -MCA (Fig. 4D,E),⁽⁴⁰⁾ may have also contributed to the inhibition of FXR signaling and thereby promoting the progression of HCC.

Knowing oxysterols can be accumulated as a result of LXR activation and *Cyp7b1* suppression,⁽²²⁾ and oxysterols can promote the recruitment of tumor-promoting myeloid cells and inhibition of DCs,⁽⁴¹⁾ we went on to measure the concentrations of cholesterol and oxysterols, including 20-HC, 22(R)-HC, 22(S)-HC, 24(R/S)-HC, 25-HC, 27-HC, and 7 α / β -HC in adjacent normal liver tissues of tumor-bearing mice. No significant change was observed in liver cholesterol level among the three genotypes (Fig. 4F). Among the oxysterol species, the hepatic levels of 27-HC, a chemotactic factor for tumor-promoting myeloid cells,⁽⁴¹⁾ were increased in both *LXR α KI* and *VP-LXR α* mice (Fig. 4G). Interestingly, the hepatic concentrations of several oxysterols, including 22R-HC and 7 α / β -HC, were decreased in both genotypes (Fig. 4G).

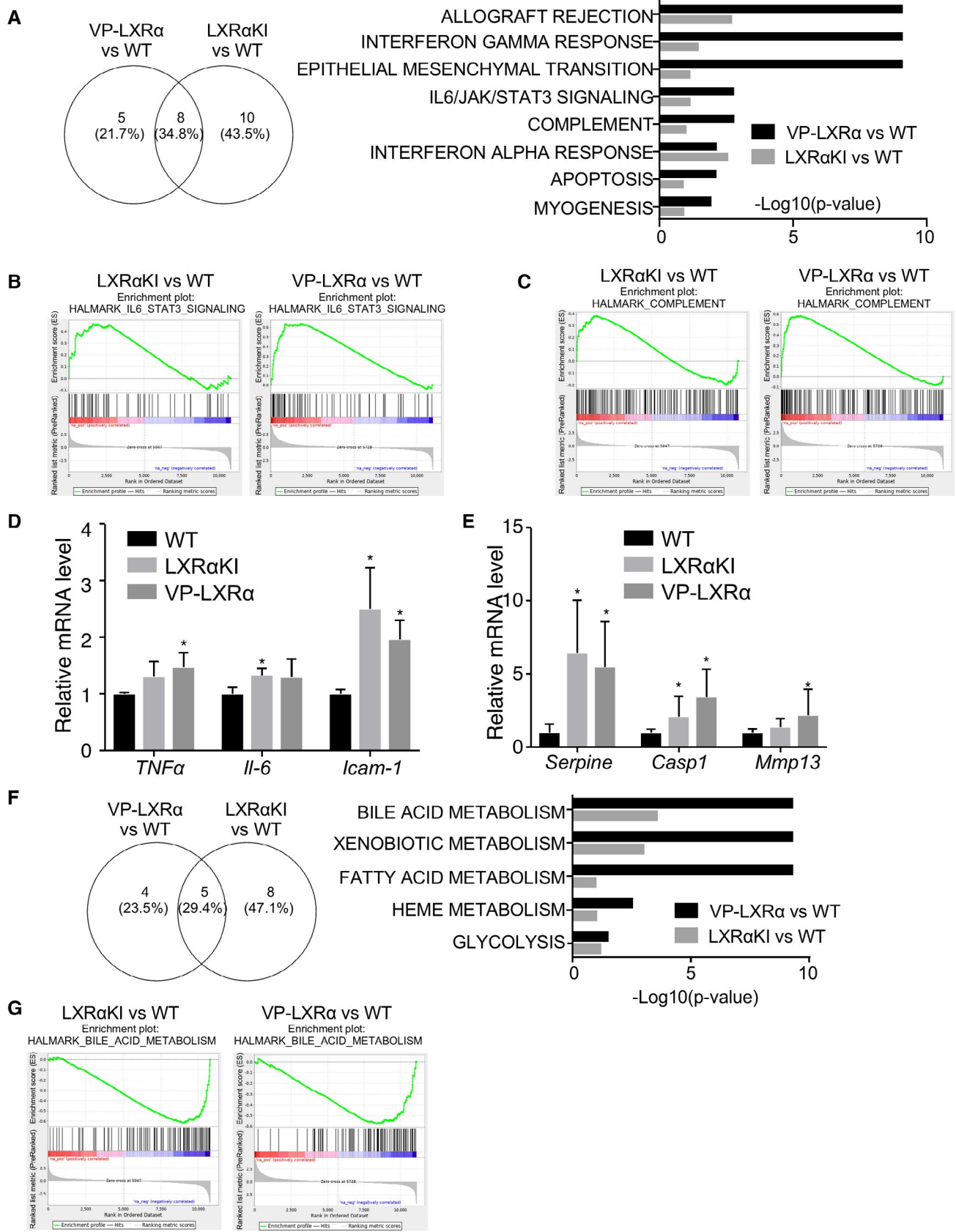


FIG. 3. Chronic activation of LXR α up-regulates pathways associated with innate immune suppression, but down-regulates the bile acid metabolism pathway in chemical-induced HCC. (A) Venn plot derived from RNA-seq analysis shows the pathways up-regulated in tumors from *LXR α KI* and *VP-LXR α* transgenic mice as compared with WT mice. Eight commonly up-regulated pathways are shown on the right. (B,C) GSEA for HALMARK_IL6_JAK_STAT3_SIGNALING (B) and HALMARK_COMPLEMENT (C) in tumors derived from *LXR α KI* (left panels) and *VP-LXR α* (right panels) mice as compared with WT mice. (D,E) The tumor mRNA expression of representative genes in the IL-6/JAK/STAT3 signaling pathway (D) and complement pathway (E). (F) Venn plot derived from RNA-seq analysis shows the pathways down-regulated in tumors from *LXR α KI* and *VP-LXR α* mice as compared with WT mice. Five pathways commonly down-regulated are shown on the right. (G) GSEA for HALMARK_BILE_ACID_METABOLISM in tumors from *LXR α KI* (left) and *VP-LXR α* (right) mice (n = 6 for each group). **P* < 0.05, compared with WT groups in (D) and (E).

CHEMICAL-INDUCED HCC IN LXR α -ACTIVATED MICE IS ACCOMPANIED BY UP-REGULATION OF MO-MDSCS AND DOWN-REGULATION OF CYTOTOXIC T CELLS AND DENDRITIC CELLS

Because activation of the IL-6/JAK/STAT3 signaling pathway and the complement system are closely related to the recruitment of MDSCs and escape of immune surveillance,⁽³⁵⁾ and the hepatic accumulation of 27-HC can function as a chemotactic factor to recruit tumor-promoting myeloid cells,⁽⁴¹⁾ we went on to determine whether activation of LXR α affected tumor infiltration of immune cells. Compared with WT mice, *LXR α KI* and *VP-LXR α* mice showed increased tumor infiltration of CD45⁺ cells as shown by immunohistochemistry (Supporting Fig. S3A). We then used flow cytometry to profile the intratumor immune cells with the gating strategies outlined in Supporting Fig. S3B. Our flow cytometry results revealed that both *LXR α KI* and *VP-LXR α* mice showed (1) a reduced number of cytotoxic CD8⁺ T cells, but no change in CD4⁺ T cells (Fig. 5A); (2) a decreased number of total DCs (Fig. 5B) and CD103⁺DCs (Fig. 5C) who transport intact antigens to the lymph nodes and prime tumor-specific CD8⁺ T cells,^(42,43) but no decrease in the total number of macrophages (Fig. 5B) or changes in the number of CD206⁺ macrophages (also known as alternatively activated macrophage, or M2 macrophages)⁽⁴⁴⁾ (Fig. 5D); and (3) an induction of the tumor-promoting Mo-MDSCs, but not the G-MDSCs (Fig. 5E).

Next, we wanted to determine the mechanism by which activation of LXR α promotes Mo-MDSC recruitment. It has been reported that the oxysterol-CXC chemokine receptor 2 (CXCR2) axis plays

a key role in the recruitment of tumor-promoting CD11b⁺Gr-1⁺ myeloid cells. Specifically, tumor-derived oxysterols, such as 27-HC, function as chemotactic factors for the migration of CXCR2-expressing CD11b⁺Gr-1⁺ myeloid cells.⁽⁴¹⁾ Our flow cytometry analysis revealed an increased number of CXCR2⁺ Mo-MDSCs in the liver tumor tissues, but not in adjacent nontumor tissues (Fig. 5F), consistent with the accumulation of 27-HC in *LXR α KI* and *VP-LXR α* mice (Fig. 4G). Because Mo-MDSCs are derived from CXCR2⁺ GMPs,⁽⁴⁵⁾ we measured the CXCR2⁺ GMPs isolated from the bone marrow of tumor-bearing *LXR α KI* and *VP-LXR α* mice by flow cytometry. As shown in Fig. 5G, increased numbers of CXCR2⁺ GMPs were observed in both *LXR α KI* and *VP-LXR α* mice.

Taken together and as summarized in Fig. 5H, our current study has shown that chronic activation of LXR α promotes DEN/TCPOBOP-induced HCC by (1) promoting innate immune suppression by increased recruitment of MDSCs and reduced number of cytotoxic CD8⁺ T cells and DCs by enhancing the oxysterols-CXCR2 signaling pathway; and (2) accumulation of pro-HCC secondary bile acids, including ω -MCA, HDCA, T-DCA, and T-UDCA, as a result of Cyp7a1 activation.

CHRONIC ACTIVATION OF LXR α SENSITIZES MICE TO MYC-DRIVEN HCC

We then used the *LAP-MYC* transgenic mice to determine whether chronic activation of LXR α also sensitizes mice to oncogene-driven liver carcinogenesis. The *LAP-MYC* transgenic mice express the c-MYC oncogene in hepatocytes under the control of the hepatocyte-specific *LAP* gene promoter.⁽²³⁾ In this experiment, the *LXR α KI* allele was bred into the *LAP-MYC* transgenic background as outlined in

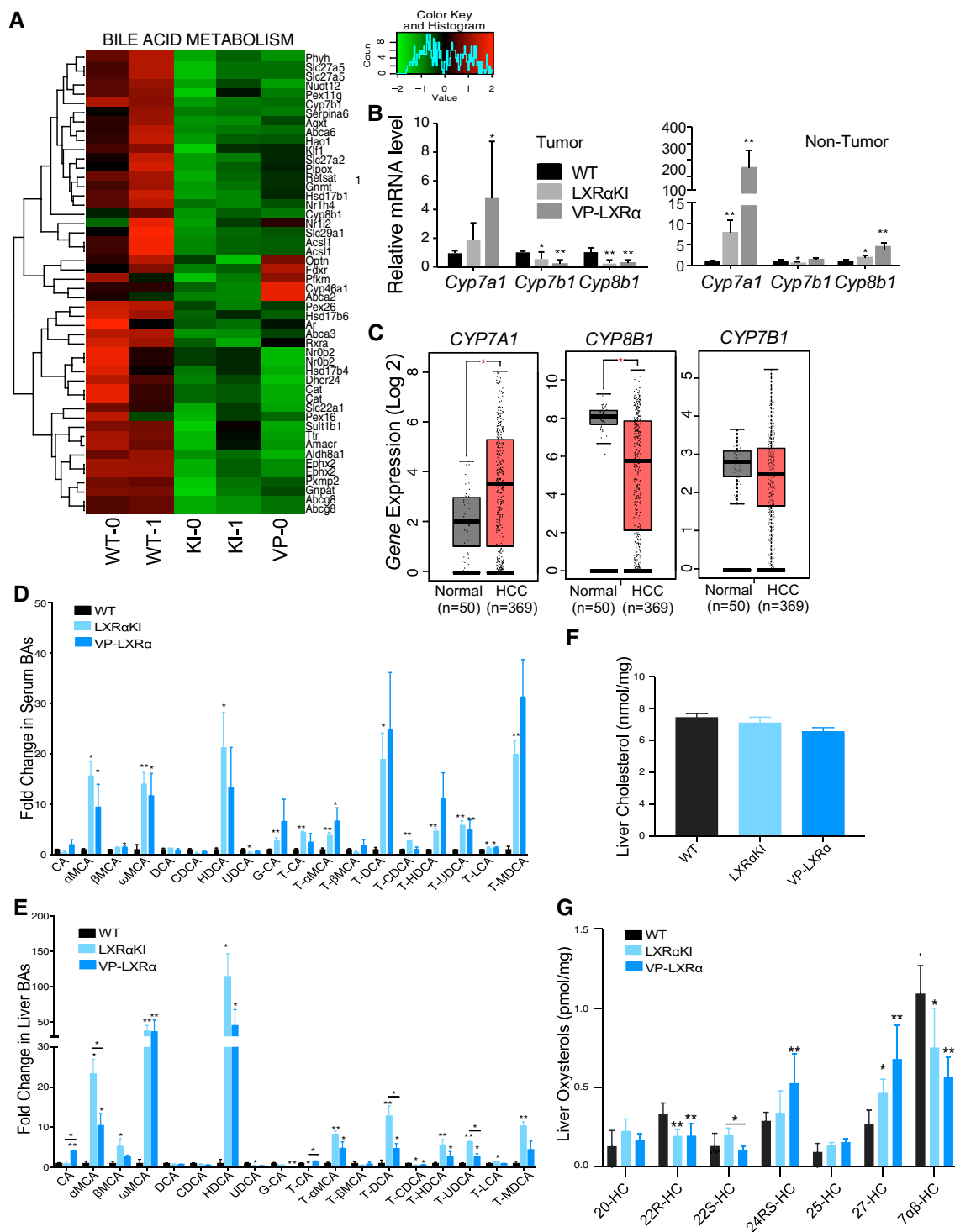


FIG. 4. Chronic activation of LXR α accumulates pro-HCC bile acid species and oxysterols in chemical-induced HCC. (A) Heatmap of gene expressions in the bile acid metabolism pathway. Each column represents individual mice. (B) The tumor (top) and nontumor (bottom) tissue mRNA expression of *Cyp7a1*, *Cyp7b1*, and *Cyp8b1* was measured by real-time PCR. (C) Analysis of *CYP7A1*, *CYP7B1*, and *CYP8B1* gene expression from the TCGA HCC data set (normal control n = 50; HCC n = 369). (D,E) Relative levels of bile acids in the serum (D) and liver tissues (E) of tumor-bearing WT, *LXR α KI*, and *VP-LXR α* mice. (F,G) The liver concentrations of cholesterol (F) and oxysterols (G) (n = 3–6 for each group). * $P < 0.05$; ** $P < 0.01$. Abbreviation: a-MCA, a-muricholic acid; BA, bile acid; b-MCA, b-muricholic acid; CDCA, chenodeoxycholic acid; DCA, deoxycholic acid; G-CA, glycocholic acid; HC, Hydroxycholesterol; T-murideoxycholic acid; T-aMCA, tauro-a-muricholic acid; T-b-MCA, tauro-b-muricholic acid; T-CA, taurocholic acid; T-CDCA, taurochenodeoxycholic acid; T-HDCA, taurohyodeoxycholic acid; T-LCA, tauroolithocholic acid; T-MDCA, T-murideoxycholic acid; and UDCA, ursodeoxycholic acid.

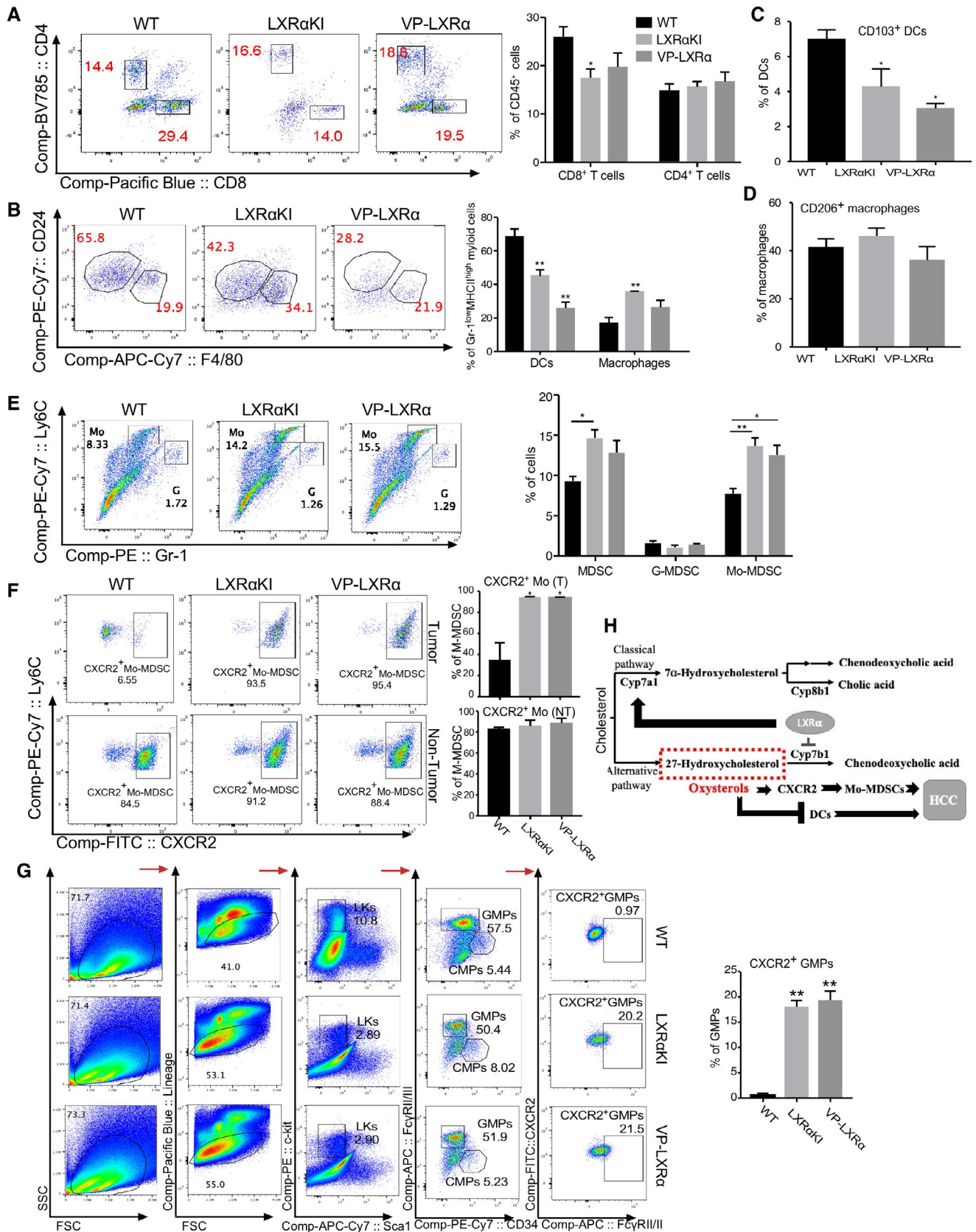


FIG. 5. Chemical-induced HCC in $LXR\alpha$ -activated mice is accompanied by up-regulation of Mo-MDSCs and down-regulation of cytotoxic T cells and DCs. (A-G) Flow cytometry analysis of tumor tissues derived from WT, $LXR\alpha KI$, and $VP-LXR\alpha$ mice. Shown are representative density plots (left) and quantification (right) of $CD45^+CD8^+CD4^-$ T cells and $CD45^+CD8^-CD4^+$ T cells in tumor tissues (A); representative density plots (left) and quantification (right) of $CD45^+Gr-1^{low}MHCII^{high}CD11b^+F4/80^-$ myeloid cells (DCs) and $CD45^+Gr-1^{low}MHCII^{high}CD11b^+F4/80^+$ myeloid cells (macrophages) (B); quantification of $CD103^+$ DCs (C); quantification of $CD206^+$ macrophages (D); representative density plots (left) and quantification (right) of $CD45^+CD11b^+Gr-1^+$ myeloid cells (total MDSCs), $CD45^+CD11b^+Gr-1^{high}$ myeloid cells (G-MDSCs), and $CD45^+CD11b^+Gr-1^{int}$ myeloid cells (Mo-MDSCs) (E); quantification of $CXCR2^+$ Mo-MDSCs in tumors (top) and nontumor tissues (bottom) (F); and quantification of $CXCR2^+$ GMPs ($CD45^+Lin^-c-Kit^{high}Sca1^-FcyRII/III^{high}CD34^+$) in the bone marrows (G). (H) Proposed role of $LXR\alpha$ in promoting oxysterol accumulation and innate immune suppression. Results are presented as mean \pm SEM (n = 3 for each group). * $P < 0.05$; ** $P < 0.01$. Abbreviation: FITC, fluorescein isothiocyanate; G-MDSC, granulocyte-like myeloid derived suppressor cells; and Mo-MDSC, monocytic myeloid-derived suppressor cells.

Fig. 6A, and the liver cancer phenotype in the resultant $LAP-MYC/LXR\alpha KI$ mice was compared with that of the $LAP-MYC$ transgenic mice. The $LAP-MYC$ and $VP-LXR\alpha KI$ alleles were independently genotyped by PCR (data not shown). The tumor growth *in vivo* was monitored by ultrasound imaging starting from 5 weeks of age. At 14 weeks of age, $LAP-MYC/LXR\alpha KI$ male mice exhibited severe abdominal distension indicative of extensive tumor burden, as shown by representative sonograph in Fig. 6B. Mice were sacrificed at 14 weeks of age, at which the liver to body weight ratio was higher in $LAP-MYC/LXR\alpha KI$ mice (Fig. 6C). Increased liver tumorigenesis in $LAP-MYC/LXR\alpha KI$ mice was confirmed by gross appearance of the liver (Fig. 6D), as well as quantifications of tumor incidence (Fig. 6E) and tumor multiplicity (Fig. 6F).

RNA-seq analysis on liver tumor tissues revealed that compared with the $LAP-MYC$ mice, $LAP-MYC/LXR\alpha KI$ mice had up-regulation of the IL-6-JAK-STAT3 and complement pathways (Fig. 6G), consistent with the DEN/TOPOBOP model. Interestingly, the intratumor expression of *Cyp7a1* and *Cyp7b1/Cyp8b1* was suppressed and induced, respectively (Fig. 6H), a pattern opposite to the chemical model. GSEA analysis showed the bile acid metabolism pathway was up-regulated (Fig. 6I), which was also opposite to the chemical model.

Discussion

The pathophysiological function of $LXR\alpha$ and $LXR\beta$ in the development of HCC remains controversial. A better understanding of the role of LXRs in liver carcinogenesis will help to develop HCC therapeutics that target LXRs. Activation of $LXR\beta$ was reported to inhibit cancers by reducing MDSC

recruitment in multiple murine cancer models and patients.⁽¹⁵⁾ Based on the widely held presumption that $LXR\alpha$ and $LXR\beta$ share similar functions, we initially speculated that chronic activation of $LXR\alpha$ may inhibit hepatocarcinogenesis. To our surprise, we found that the expression of $LXR\alpha$, but not $LXR\beta$ was elevated in patients with HCC compared to patients with CC. Further studies found that the expression of $LXR\alpha$ in the development of HCC was dynamic, and increased expression of $LXR\alpha$ was found in advanced HCC compared with pre-neoplastic hyperplastic livers. In our preclinical models, chronic activation of $LXR\alpha$ systematically or hepatocyte specifically was sufficient to sensitize mice to HCC induced by DEN/TCPOBOP or the *c-MYC* oncogene.

LXRs have been proposed to be therapeutic targets for several cancer types, including HCC.⁽¹¹⁻¹³⁾ We reason that the discrepancies between our results and previous reports are likely due to the isoform specific effect of LXR on carcinogenesis. Most of the LXR ligands that were used to show the anti-cancer effects of LXR, such as RGX104, T0901317 and GW3965, can activate both the α and β isoforms. In the reported HCC studies, the authors either did not design experiments that differentiate the effect of the two LXR isoforms,^(11,12) or the isoform effect was shown on the regulation of certain genes, but not the HCC growth.⁽¹³⁾ In the non-HCC cancer studies, the authors used either RGX104 in $LXR\alpha$ null mice to conclude the effect of $LXR\beta$ activation,⁽¹⁵⁾ or they used melanoma cells that predominantly express $LXR\beta$.⁽⁴⁶⁾ In the current study and using our genetic models that bear the exclusive activation of $LXR\alpha$, we showed that chronic activation of $LXR\alpha$ sensitized mice to hepatocarcinogenesis. The expression of $LXR\beta$ was not affected by the transgenic expression of $VP-LXR\alpha$, suggesting that the phenotype was not due to dysregulation of $LXR\beta$ in our $LXR\alpha$ -activated

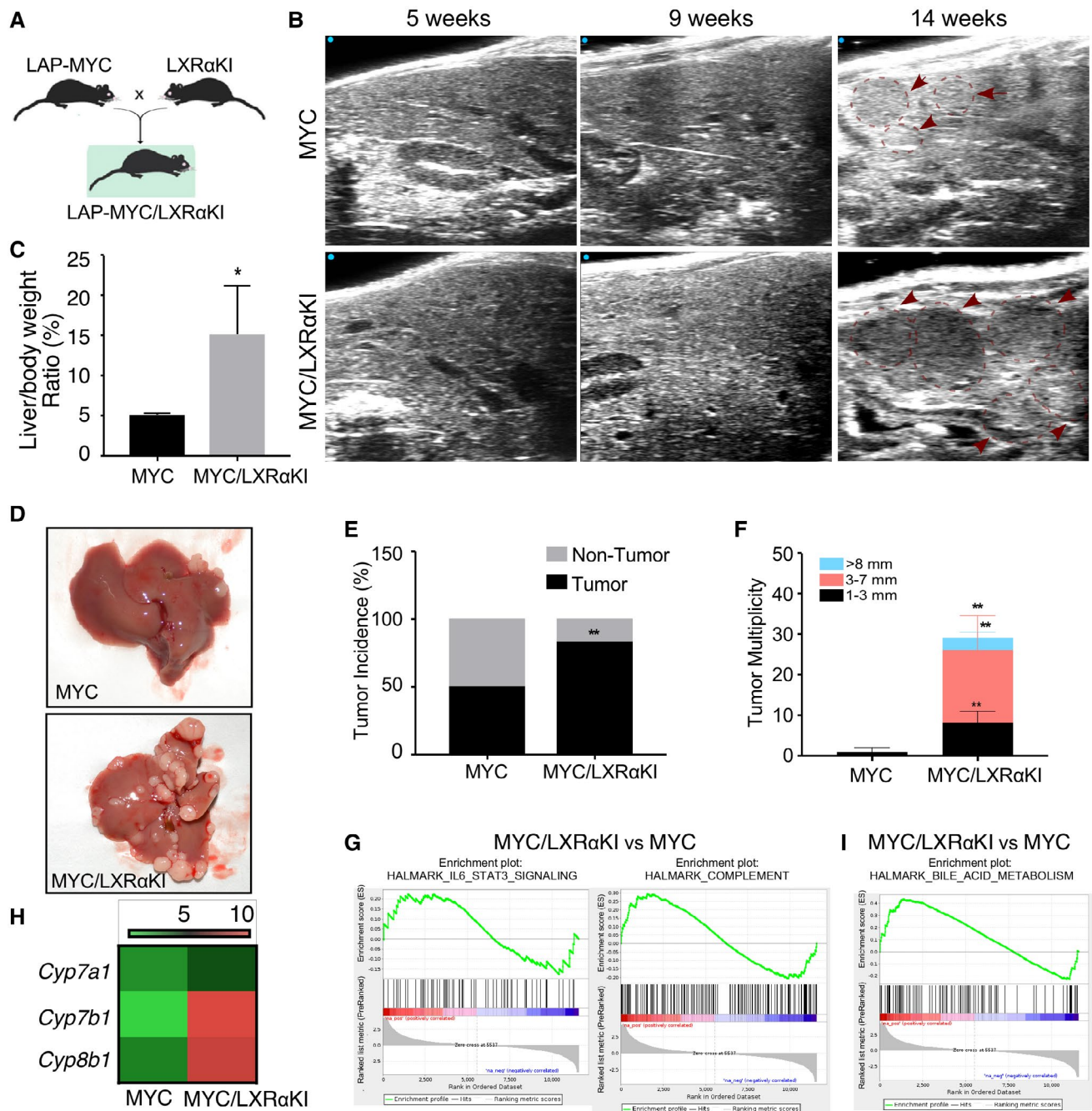


FIG. 6. Chronic activation of LXR α sensitizes mice to MYC-driven HCC. (A) Schematic representation of the crossbreeding between *LAP-MYC* transgenic mice and *LXRAKI* mice to generate the *LAP-MYC/LXRAKI* mice. (B) Representative sonographs at indicated time points. Dotted circles indicate tumor nodules. Arrowheads indicate acoustic halos surrounding the large tumor nodules. (C) Liver to body weight ratio. (D) Representative gross appearance of tumor-bearing livers of mice at 14 weeks of age. (E,F) Liver tumor incidence (E) and multiplicity (F) were calculated. (G) GSEA for HALMARK_IL6_STAT3_SIGNALING (left) and HALMARK_COMPLEMENT (right). (H) Heatmap of gene expression of *Cyp7a1*, *Cyp7b1*, and *Cyp8b1*. (I) GSEA for HALMARK_BILE_ACID_METABOLISM. Results are presented as mean \pm SEM ($n = 3-5$ for each group). * $P < 0.05$; ** $P < 0.01$, compared with the *LAP-MYC* group.

models. Future studies are necessary to determine whether ligand-dependent activation of LXR α will have the same sensitizing effect as the genetic activation. For example, we could conduct studies on LXR β null mice challenged with the TCPOBOP/DEN model in the presence or absence of RGX-104 treatment, or we could introduce the Myc transgene into the LXR β knockout background before treating them with RGX-104. The mechanisms for the isoform specific effect of LXRs on HCC or other cancer types remain to be understood.

LXRs were previously shown to promote cholesterol catabolism to form bile acids in mice by inducing *Cyp7a1* and suggested to promote the accumulation of oxysterols by suppressing the expression of *Cyp7b1*.⁽²²⁾ In our current models, we found the expression of *Cyp7a1* was indeed induced, which may explain the accumulation of bile acids, including several secondary bile acid species known to be pro-HCC. We also found the expression of *Cyp7b1* was suppressed by chronic activation of LXR α when mice were challenged with the DEN/TCPOBOP model. The suppression of *Cyp7b1* may have explained the accumulation of oxysterols, including 27-HC, in DEN/TCPOBOP-treated LXR α KI and VP-LXR α mice.

The immune cell profiling results in our LXR α activation models were intriguing. Activation of LXR β was reported to reduce MDSC recruitment in multiple cancer types, which was reasoned to be responsible for the cancer inhibitory activity of LXR β .⁽¹⁵⁾ However, we showed that activation of LXR α was associated with a higher abundance of Mo-MDSCs and reduced numbers of cytotoxic T cells and DCs in tumors of LXR α KI and VP-LXR α mice. Further analysis revealed a higher CXCR2 gene expression and a higher number of CXCR2+ Mo-MDSCs in LXR α KI and VP-LXR α tumors. The increased recruitment of Mo-MDSCs to LXR α -activated liver tumors may be explained by the accumulation oxysterols, such as 27-HC, which can function as a chemotactic factor to recruit tumor-promoting myeloid cells.⁽⁴¹⁾ The up-regulation of IL-6/JAK/STAT3 signaling and complement pathways in tumor-bearing LXR α -activated livers may have also contributed to the induction of innate immune suppression.^(35,36) Meanwhile, the accumulation of oxysterols may have contributed to the activation of the IL-6/JAK/STAT3 signaling pathway, as oxysterols, such as 27-HC, have been reported to

promote the accumulation of cellular reactive oxygen species and subsequent activation of the IL-6/STAT3 signaling pathway.⁽⁴⁷⁾ Nevertheless, we observed an increased number of CXCR2+ GMPs, precursors of Mo-MDSCs,⁽⁴⁵⁾ in the bone marrow of LXR α KI and VP-LXR α mice, which helped to explain the elevation of Mo-MDSCs but not G-MDSCs. However, the mechanism linking LXR α activation and increased GMP surface expression of CXCR2 remains to be defined. Future studies are necessary to understand the discrepancy between the effects of LXR α activation and LXR β activation on MDSC recruitment. In our models, LXR α was specifically and constitutively activated. In contrast, the reported LXR β effect on MDSC recruitment relied on a pharmacological activation of LXR β in LXR α knockout mice, in which the effect of LXR α ablation on the phenotypic exhibition cannot be excluded.^(15,46)

Although chronic activation of LXR α sensitized mice to both the DEN/TCPOBOP and c-MYC models of HCC, these two models exhibited overlapping yet distinct mechanistic insights. The liver tumor tissues from both models showed shared up-regulation of the IL-6-JAK-STAT3 and complement pathways. However, the pattern of *Cyp7a1* and *Cyp7b1/Cyp8b1* regulation was opposite between these two models. GSEA analysis showed that the bile acid metabolism pathway was suppressed and up-regulated in the DEN/TCPOBOP and c-MYC models, respectively. The differences may be explained by the fact that these are two HCC models of distinct mechanisms. Driven by a potent oncogene, the LAP-MYC model is more aggressive than the DEN/TCPOBOP model in terms of tumor development and overall tumor burden. Our analysis of the clinical samples suggested that the effect of LXR α on the development of HCC could be stage-specific.

Among the limitations, we recognized that our findings of increased IL-6/STAT3 and complement pathways, and altered bile acid metabolism in the chemical model of HCC, are associations. Although the increased IL-6/STAT3 and complement pathways were also observed in the c-Myc model, the dependence of these pathway changes on the HCC phenotype remains to be experimentally verified. For example, it will be interesting to know whether IL-6 deletion or neutralization will abolish the LXR α activation-responsive hepatocarcinogenesis in both the chemical and c-Myc models.

In summary, we have uncovered a role of *LXR α* in the development of HCC. Chronic activation of *LXR α* promotes HCC, at least in part, by promoting innate immune suppression as a result of accumulation of oxysterols, as well as up-regulation of the IL-6/JAK/STAT3 signaling and complement pathways. Our results suggest that cautions need to be applied when LXR-activating drugs are explored for their use in HCC treatment.

Acknowledgment: Wen Xie is supported in part by the Joseph Koslow Endowed Professorship provided by the University of Pittsburgh School of Pharmacy. The authors thank Laura Dubois for the sample preparation, data collection, data analysis, and report writing; J. Will Thompson and Matt Foster for the data analysis and report review; and Arthur Moseley for the scientific oversight, at the Duke University School of Medicine, for the use of the Proteomics and Metabolomics Shared Resource, which provided the service of oxysterol analysis.

REFERENCES

- Sukowati CH, El-Khobar KE, Ie SI, Anfuso B, Muljono DH, Tiribelli C. Significance of hepatitis virus infection in the oncogenic initiation of hepatocellular carcinoma. *World J Gastroenterol* 2016;22:1497-1512.
- Poon D, Anderson BO, Chen L-T, Tanaka K, Lau WY, Van Cutsem E, et al. Management of hepatocellular carcinoma in Asia: consensus statement from the Asian Oncology Summit 2009. *Lancet Oncol* 2009;10:1111-1118.
- Villanueva A. Hepatocellular carcinoma. *N Engl J Med* 2019;380:1450-1462.
- Huang W, Zhang J, Washington M, Liu J, Parant JM, Lozano G, et al. Xenobiotic stress induces hepatomegaly and liver tumors via the nuclear receptor constitutive androstane receptor. *Mol Endocrinol* 2005;19:1646-1653.
- Marcu KB, Bossone SA, Patel AJ. Myc function and regulation. *Annu Rev Biochem* 1992;61:809-860.
- Repa JJ, Mangelsdorf DJ. The liver X receptor gene team: potential new players in atherosclerosis. *Nat Med* 2002;8:1243-1248.
- Hutchinson SA, Lianto P, Moore JB, Hughes TA, Thorne JL. Phytosterols inhibit side-chain oxysterol mediated activation of LXR in breast cancer cells. *Int J Mol Sci* 2019;20:3241.
- Munir MT, Ponce C, Powell CA, Tarafdar K, Yanagita T, Choudhury M, et al. The contribution of cholesterol and epigenetic changes to the pathophysiology of breast cancer. *J Steroid Biochem Mol Biol* 2018;183:1-9.
- Krycer JR, Phan L, Brown AJ. A key regulator of cholesterol homeostasis, SREBP-2, can be targeted in prostate cancer cells with natural products. *Biochem J* 2012;446:191-201.
- Wan D, Yang Y, Liu Y, Cun X, Li M, Xu S, et al. Sequential depletion of myeloid-derived suppressor cells and tumor cells with a dual-pH-sensitive conjugated micelle system for cancer chemioimmunotherapy. *J Control Release* 2019;317:43-56.
- Moren A, Bellomo C, Tsubakihara Y, Kardassis D, Mikulits W, Heldin CH, et al. LXR α limits TGF β -dependent hepatocellular carcinoma associated fibroblast differentiation. *Oncogenesis* 2019;8:36.
- Bellomo C, Caja L, Fabregat I, Mikulits W, Kardassis D, Heldin CH, et al. Snail mediates crosstalk between TGF β and LXR α in hepatocellular carcinoma. *Cell Death Differ* 2018;25:885-903.
- Xiong H, Zhang Y, Chen S, Ni Z, He J, Li X, et al. Induction of SOCS3 by liver X receptor suppresses the proliferation of hepatocellular carcinoma cells. *Oncotarget* 2017;8:64083-64094.
- Wang Z, Yang X, Chen L, Zhi X, Lu H, Ning Y, et al. Upregulation of hydroxysteroid sulfotransferase 2B1b promotes hepatic oval cell proliferation by modulating oxysterol-induced LXR activation in a mouse model of liver injury. *Arch Toxicol* 2017;91:271-287.
- Tavazoie MF, Pollack I, Tanqueco R, Ostendorf BN, Reis BS, Gonsalves FC, et al. LXR/ApoE activation restricts innate immune suppression in cancer. *Cell* 2018;172:825-840 e818.
- Bovenga F, Sabba C, Moschetta A. Uncoupling nuclear receptor LXR and cholesterol metabolism in cancer. *Cell Metab* 2015;21:517-526.
- Carpenter KJ, Valfort A-C, Steinauer N, Chatterjee A, Abuirqeba S, Majidi S, et al. LXR-inverse agonism stimulates immune-mediated tumor destruction by enhancing CD8 T-cell activity in triple negative breast cancer. *Sci Rep* 2019;9:19530.
- Zelcer N, Tontonoz P. Liver X receptors as integrators of metabolic and inflammatory signaling. *J Clin Invest* 2006;116:607-614.
- Villablanca EJ, Raccosta L, Zhou D, Fontana R, Maggioni D, Negro A, et al. Tumor-mediated liver X receptor- α activation inhibits CC chemokine receptor-7 expression on dendritic cells and dampens antitumor responses. *Nat Med* 2010;16:98-105.
- A-Gonzalez N, Bensinger SJ, Hong C, Beceiro S, Bradley MN, Zelcer N, et al. Apoptotic cells promote their own clearance and immune tolerance through activation of the nuclear receptor LXR. *Immunity* 2009;31:245-258.
- Gong H, He J, Lee JH, Mallick E, Gao X, Li S, et al. Activation of the liver X receptor prevents lipopolysaccharide-induced lung injury. *J Biol Chem* 2009;284:30113-30121.
- Uppal H, Saini SPS, Moschetta A, Mu Y, Zhou J, Gong H, et al. Activation of LXRs prevents bile acid toxicity and cholestasis in female mice. *Hepatology* 2007;45:422-432.
- Nguyen L, Robinton D, Seligson M, Wu L, Li L, Rakheja D, et al. Lin28b is sufficient to drive liver cancer and necessary for its maintenance in murine models. *Cancer Cell* 2014;26:248-261.
- Schneider CA, Rasband WS, Eliceiri KW. NIH Image to ImageJ: 25 years of image analysis. *Nat Methods* 2012;9:671-675.
- Subramanian A, Tamayo P, Mootha VK, Mukherjee S, Ebert BL, Gillette MA, et al. Gene set enrichment analysis: a knowledge-based approach for interpreting genome-wide expression profiles. *Proc Natl Acad Sci U S A* 2005;102:15545-15550.
- Wan Z, Sun J, Xu J, Moharil P, Chen J, Xu J, et al. Dual functional immunostimulatory polymeric prodrug carrier with pendent indoximod for enhanced cancer immunochemotherapy. *Acta Biomater* 2019;90:300-313.
- Youn JI, Nagaraj S, Collazo M, Gabrilovich DI. Subsets of myeloid-derived suppressor cells in tumor-bearing mice. *J Immunol* 2008;181:5791-5802.
- Liu K, Yan J, Sachar M, Zhang X, Guan M, Xie W, et al. A metabolomic perspective of griseofulvin-induced liver injury in mice. *Biochem Pharmacol* 2015;98:493-501.
- Jiang C, Xie C, Li F, Zhang L, Nichols RG, Krausz KW, et al. Intestinal farnesoid X receptor signaling promotes nonalcoholic fatty liver disease. *J Clin Invest* 2015;125:386-402.
- Zhu J, Wang P, Shehu AI, Lu J, Bi H, Ma X. Identification of novel pathways in idelalisib metabolism and bioactivation. *Chem Res Toxicol* 2018;31:548-555.
- Narayanaswamy R, Iyer V, Khare P, Bodziak ML, Badgett D, Zivadinov R, et al. Simultaneous determination of oxysterols,

- cholesterol and 25-hydroxy-vitamin D3 in human plasma by LC-UV-MS. *PLoS One* 2015;10:e0123771.
- 32) Tang Z, Li C, Kang B, Gao G, Li C, Zhang Z. GEPIA: a web server for cancer and normal gene expression profiling and interactive analyses. *Nucleic Acids Res* 2017;45:W98-W102.
 - 33) Moennikes O, Loeppen S, Buchmann A, Andersson P, Ittrich C, Poellinger L, et al. A constitutively active dioxin/aryl hydrocarbon receptor promotes hepatocarcinogenesis in mice. *Cancer Res* 2004;64:4707-4710.
 - 34) Abe T, Amaike Y, Shizu R, Takahashi M, Kano M, Hosaka T, et al. Role of YAP activation in nuclear receptor car-mediated proliferation of mouse hepatocytes. *Toxicol Sci* 2018;165:408-419.
 - 35) Su YL, Banerjee S, White SV, Kortylewski M. STAT3 in tumor-associated myeloid cells: multitasking to disrupt immunity. *Int J Mol Sci* 2018;19:1803.
 - 36) Afshar-Kharghan V. The role of the complement system in cancer. *J Clin Invest* 2017;127:780-789.
 - 37) Wada T, Kang HS, Angers M, Gong H, Bhatia S, Khadem S, et al. Identification of oxysterol 7alpha-hydroxylase (Cyp7b1) as a novel retinoid-related orphan receptor alpha (RORalpha) (NR1F1) target gene and a functional cross-talk between RORalpha and liver X receptor (NR1H3). *Mol Pharmacol* 2008;73:891-899.
 - 38) Yamada S, Takashina Y, Watanabe M, Nagamine R, Saito Y, Kamada N, et al. Bile acid metabolism regulated by the gut microbiota promotes non-alcoholic steatohepatitis-associated hepatocellular carcinoma in mice. *Oncotarget* 2018;9:9925-9939.
 - 39) Ma C, Han M, Heinrich B, Fu Q, Zhang Q, Sandhu M, et al. Gut microbiome-mediated bile acid metabolism regulates liver cancer via NKT cells. *Science* 2018;360:eaan5931.
 - 40) Sayin S, Wahlström A, Felin J, Jäntti S, Marschall H-U, Bamberg K, et al. Gut microbiota regulates bile acid metabolism by reducing the levels of tauro-beta-muricholic acid, a naturally occurring FXR antagonist. *Cell Metab* 2013;17:225-235.
 - 41) Raccosta L, Fontana R, Maggioni D, Lanterna C, Villablanca EJ, Panicia A, et al. The oxysterol-CXCR2 axis plays a key role in the recruitment of tumor-promoting neutrophils. *J Exp Med* 2013;210:1711-1728.
 - 42) Salmon H, Idoyaga J, Rahman A, Leboeuf M, Remark R, Jordan S, et al. Expansion and activation of CD103(+) dendritic cell progenitors at the tumor site enhances tumor responses to therapeutic PD-L1 and BRAF inhibition. *Immunity* 2016;44:924-938.
 - 43) del Rio ML, Bernhardt G, Rodriguez-Barbosa JJ, Forster R. Development and functional specialization of CD103+ dendritic cells. *Immunol Rev* 2010;234:268-281.
 - 44) Haque ASMR, Moriyama M, Kubota K, Ishiguro N, Sakamoto M, Chinju A, et al. CD206(+) tumor-associated macrophages promote proliferation and invasion in oral squamous cell carcinoma via EGF production. *Sci Rep* 2019;9:14611.
 - 45) Han X, Shi H, Sun Y, Shang C, Luan T, Wang D, et al. CXCR2 expression on granulocyte and macrophage progenitors under tumor conditions contributes to mo-MDSC generation via SAP18/ERK/STAT3. *Cell Death Dis* 2019;10:598.
 - 46) Pencheva N, Buss CG, Posada J, Merghoub T, Tavazoie SF. Broad-spectrum therapeutic suppression of metastatic melanoma through nuclear hormone receptor activation. *Cell* 2014;156:986-1001.
 - 47) Liu J, Liu Y, Chen J, Hu C, Teng M, Jiao K, et al. The ROS-mediated activation of IL-6/STAT3 signaling pathway is involved in the 27-hydroxycholesterol-induced cellular senescence in nerve cells. *Toxicol In Vitro* 2017;45:10-18.

Supporting Information

Additional Supporting Information may be found at onlinelibrary.wiley.com/doi/10.1002/hep4.1880/supinfo.